COBEM 2023 27TH INTERNATIONAL CONGRESS OF MECHANICAL ENGENEERING

ABCM Brazilian Society of Mechanical Sciences and Engineering
27th ABCM International Congress of Mechanical Engineering
December 04-08, 2023, Florianópolis-SC, Brazil

COB-2023-1001
INVESTIGATION ON THE IMPACT OF SAND CONTROL SCREEN DIAMETER ON SCALING AND FLOW BEHAVIOR IN OIL PRODUCTION

Rodrigo Prando Pedroni
Ayrton Cavallini Zotelle
Renato do Nascimento Siqueira
Instituto Federal do Espírito Santo, Department of Mechanical Engineering, Rod. BR 101 North, km 58, São Mateus, Espírito Santo, 29932-540, Brazil.
rodrigo.pedroni@hotmail.com
ayrton.zotelle@ifes.edu.br
renatons@ifes.edu.br

Abstract. *The exploration of pre-salt reservoirs has brought new engineering challenges, especially concerning the deposition of calcium carbonate ($CaCO_3$) on completion devices. This study focuses on investigating the impact of filtering diameter of sand control screens on scaling, flow behavior, and pressure drop in the oil extraction process. The analysis is carried out through numerical simulations using Computational Fluid Dynamics (CFD) and user-defined functions (UDF). The simulations involve different stand-alone screens with varying particle capture diameters of the wire mesh. The UDF implementation covers key aspects such as particle passing or adhesion, agglomeration growth, reduction of passing diameter, and flow resistance. In the simulations, calcium carbonate particles are represented as the solid phase, while water is represented as the fluid phase. The Discrete Phase Model (DPM) is utilized to establish a two-way coupling between the particles and the fluid, enabling the investigation of particle behavior and its interaction with the flow. The results of the simulations indicate that finer screens are more effective in capturing particles but also lead to a larger pressure drop due to particle agglomeration. It also indicates the potential use of less fine screens, while taking into account the high volume of particles into the production column that may damage equipment in the initial stages of flow. The developed model offers a simplified approach that allows for the analysis of large domains, particle quantities and can provide valuable insights for the industry in screen selection and decision-making.*

Keywords: *Computational Fluid Dynamics, Calcium carbonate scaling, Sand control screens, Discrete Phase Model, User-defined functions.*

1. INTRODUCTION

Despite the growing demand for renewable energy sources, oil continues to be one of the primary energy resources in the market. Its extraction plays a crucial role in the operation and production of several industrial and everyday items, including transportation vehicles, industrial machinery, and infrastructure. Given the significance and commercial value associated with oil exploration, companies are constantly seeking for more efficient production methods and innovative solutions to address the engineering challenges involved in its extraction. Among these challenges, the deposition of inorganic salts in reservoirs and completion elements stands out as a major concern, as it can reduce oil production and adversely affect the overall efficiency (Schiavi and Hoffmann, 2015).

Oil reservoirs consist of porous rocks that require various equipment, such as sand control screens, for controlled oil extraction. These screens must possess two key properties simultaneously: they should be fine enough to retain most of the solids present in the formation, preventing excessive abrasion and wear of internal equipment, while causing minimal productivity loss due to the resistance they impose on flow (Malbrel *et al.*, 1999). Among the different sand control systems, the stand-alone technique is considered a simple, versatile, and cost-effective option compared to other available methods. It acts as the interface between the reservoir and the production zone, utilizing sets of filtration screens to reduce the concentration of particles flowing into the production column (Pessoa, 2012).

An intrinsic phenomenon in pre-salt oil extraction, due to favorable thermodynamic and fluid dynamic conditions, is the formation of calcium carbonate crystals as a result of CO_2 flashing. During this process, ions like Ca^{2+} and ${CO_3}^{2-}$, initially dissolved in brine, tend to precipitate due to the solubility reduction of CO_2, caused mainly by pressure drops in the system (Cosmo *et al.*, 2019). Once nucleated, these crystals tend to grow due to ion supersaturation and crystal size (Chen *et al.*, 1997), and to agglomerate through Brownian motion or flow-induced movements, such as turbulence, resulting in the formation of crystalline bridges due to electromagnetic forces ()Schnebelen2015. Then, these crystals can further transform into another polymorph, typically calcite, or scale when they collide with surfaces, reducing the available area for oil flow, leading to flow restrictions, operational issues, and decreased well productivity (Cruz, 2018).

The formation of calcite scale is influenced by various parameters, including crystal diameter, shape, velocity, surface roughness, attractive forces, and fluid dynamics conditions within the flow. Given the wide range of conditions involved and the industry's need for rapid results, simplifications are necessary in numerical studies aiming to develop models that capture the key aspects of scale formation.

Several researchers have been investigating new aspects and methods to enhance the prediction of $CaCO_3$ scaling. In the works conducted by Cosmo *et al.* (2019) and Zhang and Farquhar (2001), are studied the most influential parameters for calcium carbonate precipitation, such as pressure drop and chemical composition. Cruz (2018), Vieira (2021), and Poletto *et al.* (2022), utilizing the Ansys FLUENT® software with the Discrete Element Method (DEM) formulation, which allows for the calculation of particle collisions and analysis of the forces involved, modeled the process of calcium carbonate deposition. Similarly, Maciel *et al.* (2020) conducted a study using the Discrete Phase Model (DPM) methodology, describing the particles as material points and offering, besides the lower precision, faster results as it is a lighter model compared to the DEM formulation.

These analyses enhance the industry's capability to determine whether particles will precipitate or adhere to equipment surfaces, leading to scaling issues that can negatively impact production. However, there is still a need for models that can offer fast results without necessitating simulations with impractically large time steps and mesh elements for industrial applications.

In this context, the purpose of this study is to implement some key scaling events in stand-alone screens using a user-defined function (UDF), allowing to evaluate the aspects of different filtration diameters using an Euler-Lagrange approach with the Discrete Phase Model (DPM). Enabling to assess the impacts provided by the reduction of particle concentration in the production column through finer filtration mesh, against with the potential negative effects on productivity due to the increased energy required for the flow to pass through the screen structure.

2. METHODOLOGY

The developed geometry was a representative section, considering that it can be several meters long, inspired by the sand control screen and production column configuration. Among the available methods in the literature, stand-alone screens were chosen as the object of study because of two main motivating factors: its strong focus in the literature and industry, with studies aiming to understand its peculiarities and develop more advanced screens, and the possibility of using a porous jump as a geometric simplification, due to the premium screens used for particle filtration, as shown in Fig. 1.

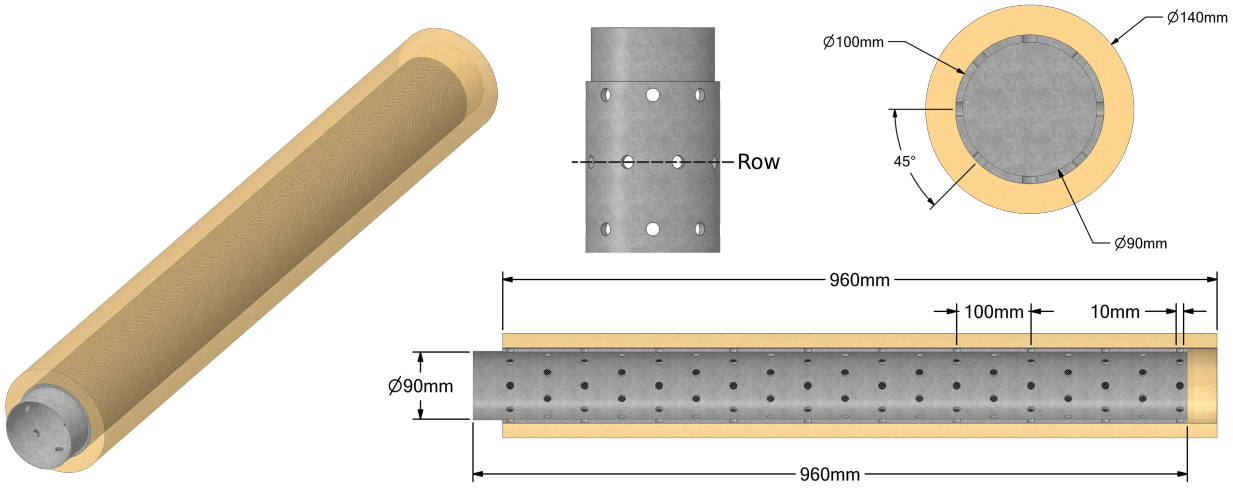

Figure 1: Geometry developed for the simulations.

To reflect real geometric proportions, the dimensions of the tube and screen were based on a commercial model available in an oil and gas wire screen catalog (Delta Screens, 2017). The pipe's internal diameter, the number, diameter and approximate distance of equidistant holes connecting the exterior to the interior of the pipe in each row were obtained from a combination of empirical data and design specifications. Additionally, were adopted the absence of the screen support and a tube length of 960 millimeters.

The construction characteristics of stand-alone screens, combined with the numerical aspects of the simulations, allowed for the simplification of using only the finest screen to represent the entire filtration system. This simplification is based on assuming that in a filtration system, the finest screen defines the maximum particle size that can pass through. Therefore, the effects of the filter screen on the flow can be represented by using the porous jump feature available in Ansys Fluent® . As porous jump is a physically based formulation that represents the resistance offered by a thin filtration media in the flow, it provides a significantly computation cost reduction.

The region around the pipe representing the reservoir near the production column was sized to encompass only the relevant volume for interaction with the filter screen, optimizing computational cost. To avoid particles escaping through the annular area opposite the inlet without interacting with the screen, a height of 20 mm was chosen for the reservoir. Furthermore, as the objective was to simulate an intermediate partition along the production column, a 40 mm displacement of the production column was applied to reduce the presence of a recirculation region close to the inlet.

A typical distribution of calcium carbonate particle diameters, obtained from the work of Vieira (2021) and illustrated in Fig. 2, was utilized as particle injection to capture the phenomenon of reduced passage diameter caused by particle accumulation on the screen surface.

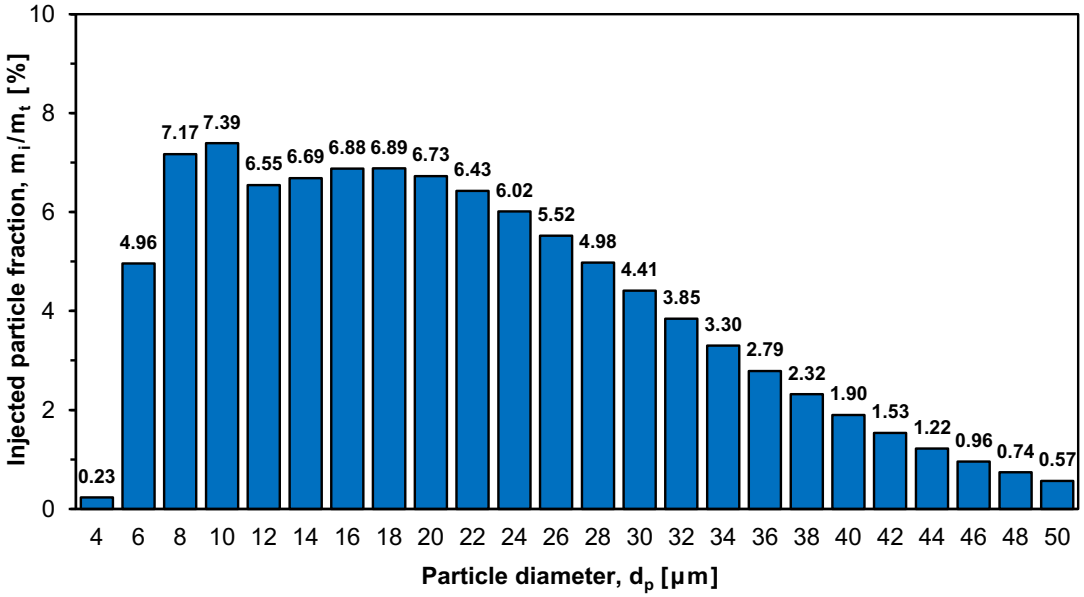

Figure 2: Particle distribution. adapted of Vieira (2021)

By selecting a particle mass flow rate of 1.374188×10^{-4} kg/s, the volumetric fraction of particles was determined to ensure that it remains below the recommended threshold of 10% by Ansys Fluent® , thereby ensuring negligible particle-particle interactions. Considering the specific mass of the particles to be 2800 kg/m^3, the volumetric fraction was calculated based on the fluid flow rate in the same inlet region as the particles, which is approximately 0.004 m^3/s. Which resulted in a value significantly lower than 10%.

Based on the analysis of the diameter distribution, three screens were selected for the study, each allowing the passage of approximately 20%, 50%, and 80% of the injected particle mass (Fig. 3). The screen diameters were chosen accordingly: 10 μm, 20 μm and 30 μm, considering that particles with diameters equal to the screen openings can pass through the screens.

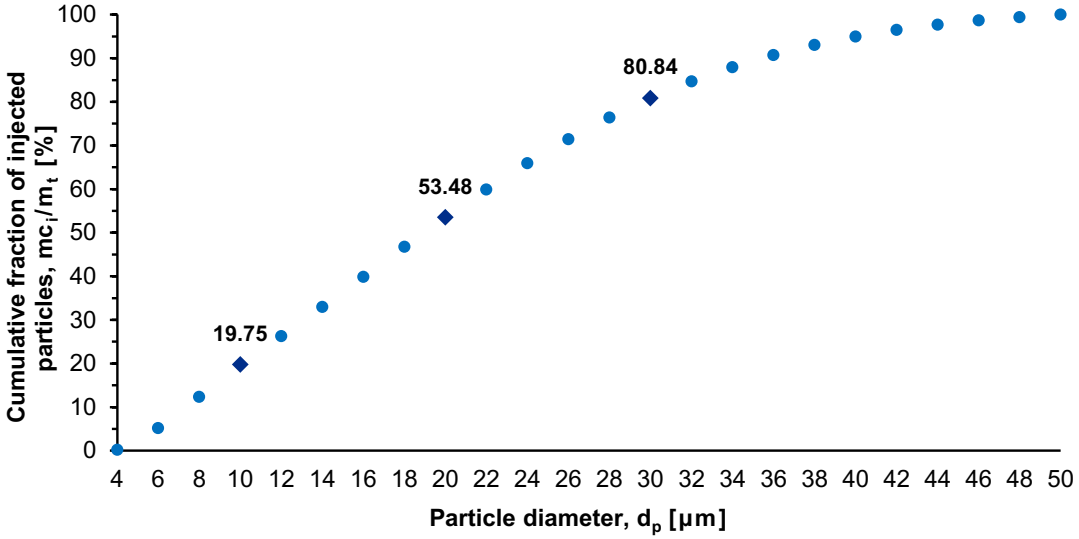

Figure 3: Accumulated mass of particles capable of passing through a screen with the corresponding filtration diameter.

To prevent particles from escaping through the annular area without interacting with the screen, the external surface of the reservoir was defined as a velocity inlet condition without particle injection (Fig. 4). By doing so, the particles are encouraged to enter the pipe through the nearest path after their entry, influenced by the resultant velocity vector of the flow. Two different boundary conditions were assigned for the outlet: in the annular region, was applied a velocity condition with the same flow as the annular inlet, and in the internal region of the tube, a pressure condition of 0 Pa. The internal region of the reservoir that does not come into contact with the pipe due to the offset was defined as a free slip wall. Except for the screen region over the connection tubes, the rest of the screen region was defined as a no-slip wall, meaning that the fluid and particles are unable to pass through these surfaces and if any particles collide with the screen region, they will adhere.

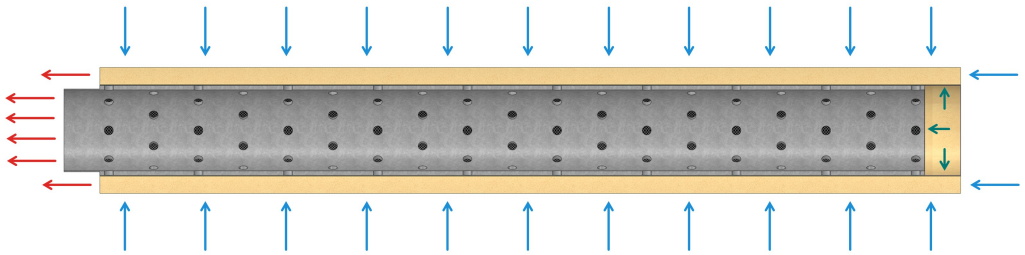

Figure 4: Representation of fluid inlet regions in blue, outlet regions in red, and free slip walls in green.

The DPM model offers the possibility of grouping particles into parcels, which are groups of particles with similar properties treated as a single entity. This reduces computational cost as a single object represents multiple particles, however, it is important to pay attention when grouping particles, as excessive grouping can affect results and lead to significant deviations in particle trajectories compared to individual analysis. In this study, it was determined that using 10 particles per parcel was suitable, considering the large number of parcels injected and the absence of significant vortices that could disperse the trajectories of grouped particles.

To capture the turbulent effects on particle displacement, the Discrete Random Walk (DRW) model was activated. This model considers turbulent variations in the flow based on the local turbulence, allowing particles to follow probabilistic trajectories that fluctuate around the streamlines.

The effects of scaling on production loss were considered by implementing subroutines in a user-defined function (UDF) that incorporates the additional pressure drop caused by scaling in the flow. This localized pressure drop influences the overall flow behavior, resulting in increased head loss and production losses. Additionally, the UDF implementation allows for the propagation of the adhered particle bed throughout the domain, beyond the immediate computational mesh vicinity of the walls, the reduction of the passage diameter due to scaling, and the re-injection of particles capable of passing through the screen on the other side.

The injection time is crucial for capturing the phenomena of interest during the simulation. A short injection time may not provide sufficient observation, while a long injection time would lead to extensive simulations with most particles exiting through the annular space, making it difficult to compare cases. Based on the domain dimensions and preliminary results, a 20 second injection time was chosen.

As particles of calcium carbonate ($CaCO_3$) adhere and accumulate on the surfaces of completion equipment, a compacted bed of particles forms, exhibiting behavior similar to a porous medium. These are permeable structures that can significantly alter flow characteristics by reducing the available space for flow. However, numerical studies that do not directly calculate the volumetric effects of particles rely on mathematical models to represent these effects.

The particle generated resistance was implemented in each mesh element using the equation developed by Ergun (1952), which describes the pressure drop caused by a porous structure that restricts flow. It was used as calibration constants A = 150 and B = 1.75, commonly found in the literature, and a sphericity of ϕ = 1. To account for the non-uniform particle distribution in the simulations, the Sauter equivalent diameter was employed (Sauter, 1926). This approach calculates an average diameter considering particle characteristics such as surface area and occupied volume, representing a mixture of particles with varying diameters as a cluster of particles with a single diameter.

The Equation 1 presents the combined equations of Sauter equivalent diameter and the Ergun equation.

$$\frac{\Delta P}{L} = A\frac{(1-\epsilon)^2\mu_f}{\phi^2\,\epsilon^3\,{d_{p,s}}^2}v + B\frac{(1-\epsilon)\rho_f}{\phi\,\epsilon^3\,d_{p,s}}v^2 \;\Leftarrow\; d_{p,s} = 6\frac{V_{t_p}}{As_{t_p}}\,. \tag{1}$$

In this equation, ΔP is the pressure drop, L is the thickness of the porous medium, ϵ is the porosity of the medium, μ_f is the viscosity of the fluid, v is the superficial velocity of the fluid, ρ_f is the specific mass of the fluid, ϕ represents the sphericity of the particles, $d_{p,s}$ is the Sauter equivalent diameter of the particles, $V_{t_p} = \sum_{i=1}^{n} N_i\,\pi\,\frac{{d_{p_i}}^3}{6}$ is the sum of the volume of all particles in the cell, and $As_{t_p} = \sum_{i=1}^{n} N_i\,\pi\,{d_{p_i}}^2$ is the sum of the surface area of all particles in the cell.

The porosity of a porous medium is influenced by various factors, including the compressibility of the structure and the diameter of the particles constituting it. In this study, the porosity of the porous medium formed by the accumulation of calcite was limited based on the findings of the study conducted by Bernabe *et al.* (1982), which investigated different porosity values for calcite under high temperature and pressure conditions. Considering that these conditions are present in petroleum reservoirs, a minimum porosity value of 0.20 was chosen based on the observations in that study.

To mathematically close the Navier-Stokes equations, the $k-\omega$ SST turbulence model was employed. This model is designed for simulations involving adverse pressure gradients near walls, which is of particular interest in scaling studies. Additionally, the $k-\omega$ SST model is capable of switching for the $k-\epsilon$ behavior in regions of free-flow, enhancing its versatility. Parameters related to algorithms, fluid, and particles can be conferred in Tab. 1 and Tab. 2.

Table 1: Parameters and algorithms used in the simulations.

Pressure-Velocity Coupling		Coupled
Spatial Discretization	Gradient	Least Squares Cell Based
	Pressure	Standard
	Momentum	First Order Upwind
	Turbulent Kinetic Energy	First Order Upwind
	Turbulence Dissipation Rate	First Order Upwind
Flow Type		Rhie-Chow: momentum-based
Transient Formulation		First Order Implicit
Time Step		0.001 seconds

Table 2: Parameters of the continuous and discrete phases.

Continuous Phase	Fluid	Water
	Specific mass	$\rho_f = 998.2\ kg/m^3$
	Viscosity	$\mu_f = 1.003 \times 10^{-3}\ Pa.s$
	Volumetric Flow Rate	$Q_f = 6.043868 \times 10^{-3}\ m^3/s$
Discrete Phase	Particles	Calcium Carbonate
	Specific mass	$\rho_p = 2800\ kg/m^3$
	Minimum Admissible Porosity	$\epsilon_{min} = 0.2$
	Particles per Parcel	10
	Mass Flow Rate	$\dot{m}_p = 1.374188 \times 10^{-4}\ kg/s$

3. RESULTS

3.1 Mesh independence test

A mesh test was conducted to ensure result independence regarding mesh refinement and determine the necessary level of refinement in the regions of main interest, as shown in Fig. 5, without unnecessarily computational costs.

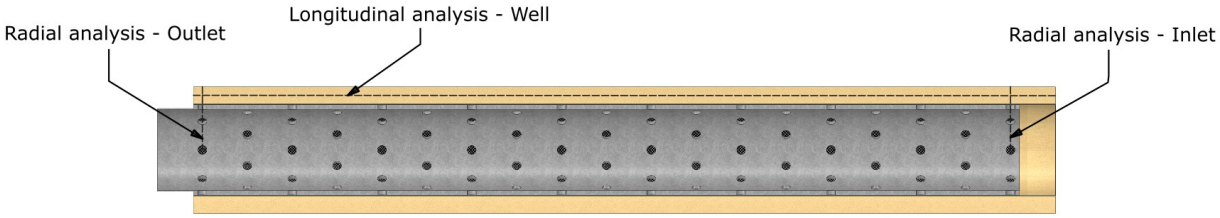

Figure 5: Line locations used for the mesh test.

Analyzing the data from all generated meshes, illustrated in Fig. 6, an assessment was conducted considering both computational cost and discrepancies between the results obtained from each mesh. The computational cost was primarily evaluated in terms of the number of elements, as the polyhedral mesh type used closely relates the number of nodes and elements.

Among the generated meshes, the mesh consisting of 1,894,932 elements showed a low variation compared to the next more refined mesh in regions of high interest and fluctuation. It also exhibited good orthogonal quality, with a minimum value of 0.20 and a maximum aspect ratio of 32, indicating its ability to accurately capture the main phenomena (Fig. 7).

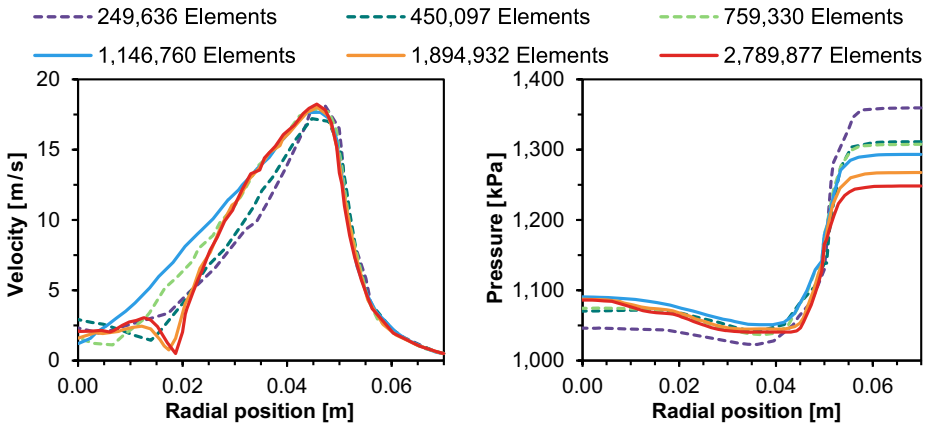

(a) Radial mesh analysis at the inlet.

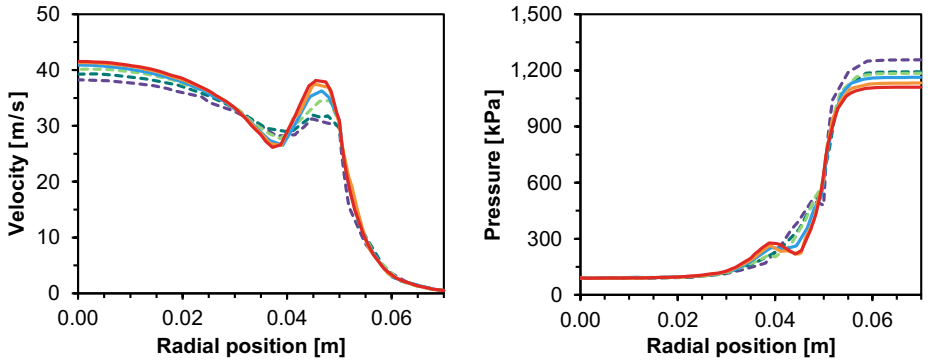

(b) Radial mesh analysis at the outlet.

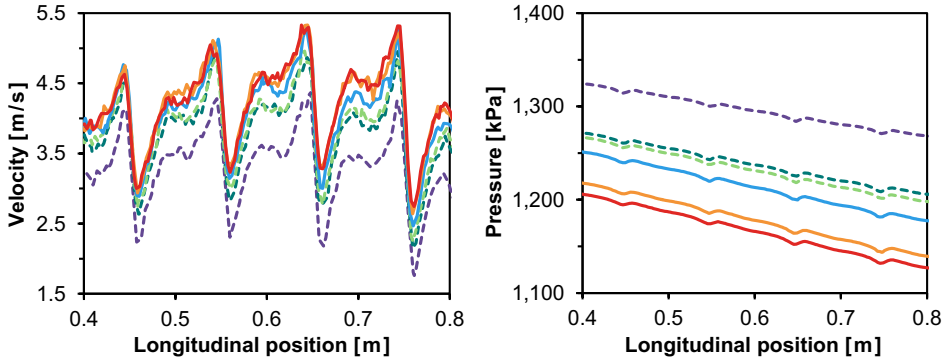

(c) Longitudinal mesh analysis in the reservoir.

Figure 6: Velocity and pressure graphs extracted in different regions of the domain.

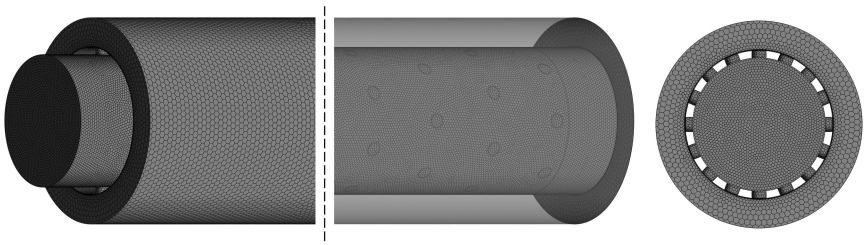

Figure 7: Resulting mesh

3.2 Calcium carbonate scaling

Figure 8 illustrates the temporal evolution of particle deposition on the 10 μm screen, revealing that particles tend to initially collide with the surfaces above the connections. This behavior is attributed to the high intensity flow directing the particles towards the interior of the pipe, where there is a considerable lower pressure due to the filtering surface between the tube and the reservoir.

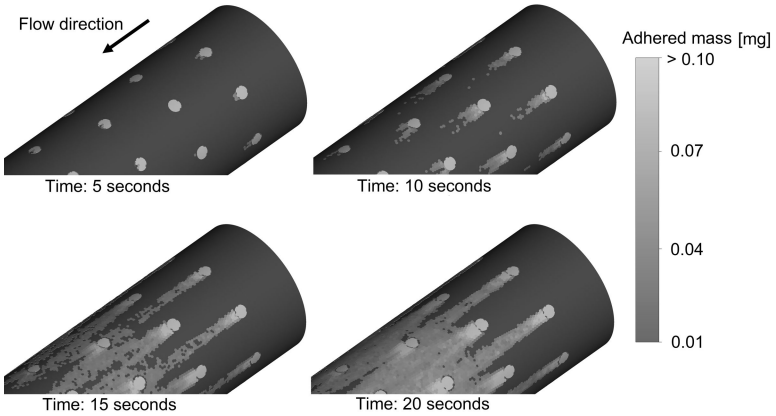

Figure 8: Adhered mass over simulation time

As the simulation progresses, the wall region begins to accumulate a significant amount of deposited mass. This phenomenon occurs as the previously available flow passages, which offered the path of least resistance, become obstructed. As a result, particles experience a less intense change in their trajectories, leading to collisions in regions downstream of the connections rather than directly at the connections themselves.

By analyzing the total deposited mass in each region at the end of the simulations, it is evident that there is a significantly higher mass of particles adhered to the connections compared to the pipe wall. This difference gradually decreases as the screen capture size increases, as shown in Table 3.

Table 3: Particles adhered mass.

Case	**Connection adhered mass [g]**	**Wall adhered mass [g]**
10 μm screen	1.75	0.97
20 μm screen	1.63	0.94
30 μm screen	1.31	0.81

The small variation observed between the 20 μm and 10 μm screen cases indicates that the flow pattern is relatively similar for all screens. Additionally, there is a trend suggesting that if the simulation of the 30 μm screen were run for a longer duration, it would likely accumulate a close amount of deposited mass in each region.

An aspect of the geometry analyzed is its ability to effectively demonstrate the impact of particle accumulation on flow behavior. The increased flow resistance caused by the obstruction of the initial connection region within the pipe leads to the diversion of flow towards other regions with lower resistance further downstream, as illustrated in Fig. 9.

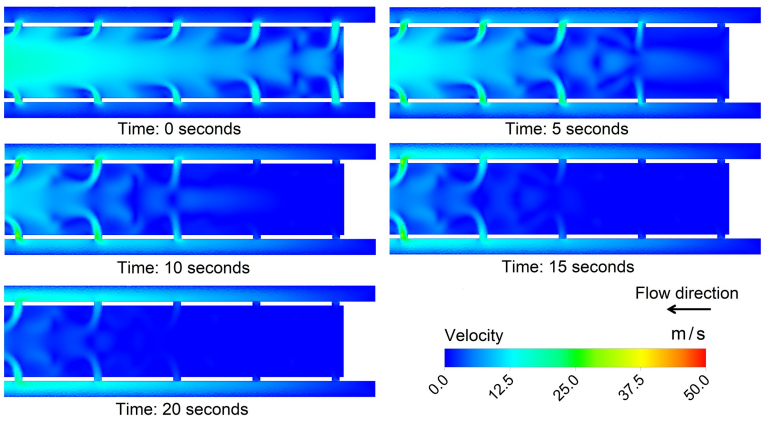

Figure 9: Velocity contours for the 20 μm screen during the simulation.

The redistribution of flow caused by particle accumulation in the obstructed region introduces complexity to flow behavior and particle adhesion. The velocity at which particles approach the screen is influenced by the degree of particle accumulation in that region, as mentioned previously, affecting the deposition patterns throughout the domain.

After the simulations were completed, velocity contours in all cases were analyzed using a vertical plane, as used in Fig. 9. This plane passes through the center of the geometry and divides it symmetrically, as shown in Fig. 10.

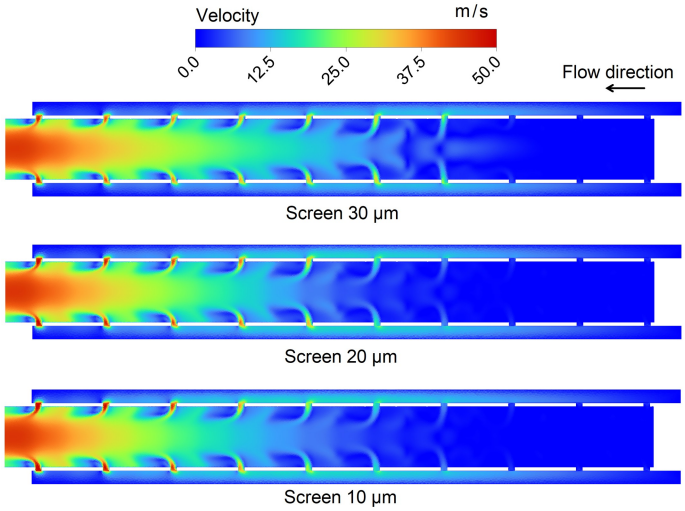

Figure 10: Velocity contours at the 22 seconds for each screen, with capture diameters of 10 μm, 20 μm, and 30 μm.

Upon analyzing Fig. 10, a significant difference in velocity contours between the 30 μm and 20 μm cases was evident. The increased capture capability of the 20 μm screen leads to a larger accumulation of particles on its surface, as particles larger than the mesh opening are unable to pass through. This accumulation creates additional obstacles and increases flow resistance, resulting in notable alterations in flow patterns and velocity distribution around the screen.

When comparing the cases with capture diameters of 20 μm and 10 μm, only a slight variation in velocity contours was observed, despite both cases capturing approximately 30% more mass compared to the less refined screen (Fig. 3). This can be attributed to the additional filtration phenomenon occurring, which is the formation of a particle filtering layer on the screen surface. This accumulated layer obstructs the passage regions, allowing only very small particles to flow through the screen. As a result, both cases converge to a similar flow regime, resulting in similar velocity contours.

By collecting data at 0.5 second intervals during the simulation, graphs were generated to illustrate the temporal evolution of particle counts in different conditions, such as suspended, adhered and leaving the domain, shown in Fig. 11.

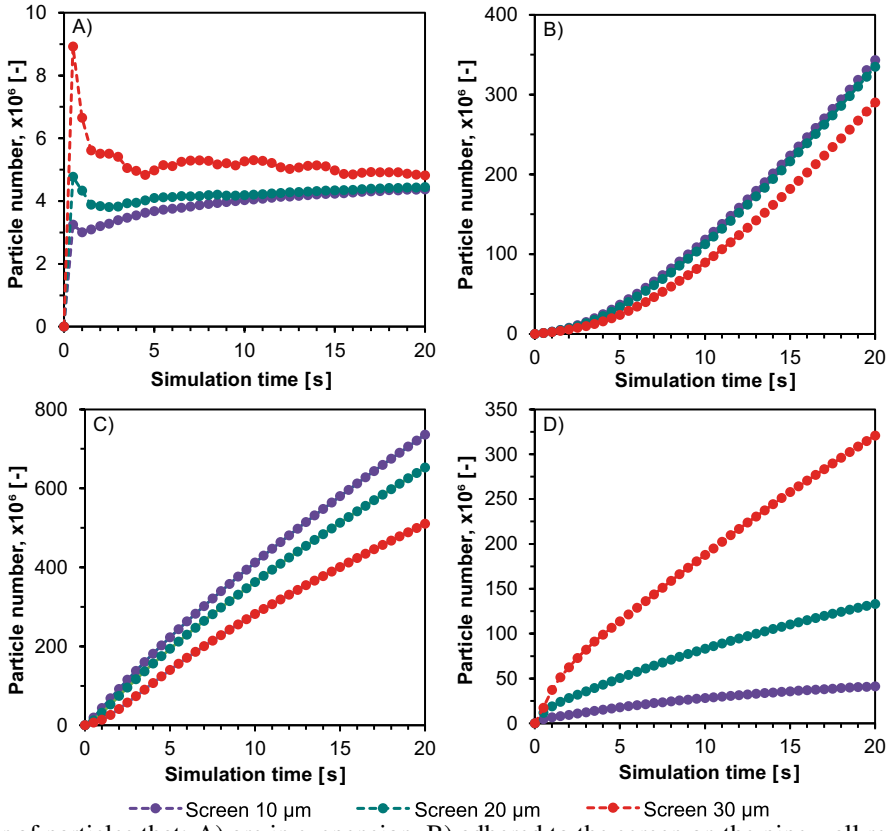

Figure 11: Number of particles that: A) are in suspension, B) adhered to the screen on the pipe wall region, C) adhered to the screen on the connection region, D) exited the domain through the production column, extracted every 0.5 seconds.

Figure 11 A exhibits an initial peak in the number of suspended particles during the early stages of the simulation. This peak can be attributed to the majority of particles passing through the initial rows and entering the interior of the pipe within this initial period. It's worth noting that the peak is lower in cases where the screen is more refined, indicating that a greater proportion of particles are retained at the screen surface.

As the simulation progresses, the screens accumulate particles on their surfaces, resulting in a decrease in the number of suspended particles over time. This accumulation prevents smaller particles from passing through to the interior of the pipe, leading to a change in the flow pattern.

As particles continue to advance through the domain searching for alternative pathways, as shown in Fig. 9, the likelihood of collision with the screen on the pipe wall increases. This is influenced by the presence of reduced radical velocity gradients, due to particle resistance, and the expanding available wall region due to scaling effects. As a result, the curve in Fig. 11 B shows an inclination, indicating an increasing trend in the number of particles adhering to the screen on the pipe wall with time.

Despite the different capture diameters used throughout the simulation, the curves for particles adhered to the screen in the connection region show a strong tendency to linearize (Fig. 11 C). This is because particles continue to collide in the region with a capture diameter of 0 μm, leading to the formation of a porous medium on the screen. This results in a consistent scaling rate, regardless of the changes in the capture diameter. This condition is predominant in most of the domain, as a significant number of particles adhere and completely block the screen passages, creating a high resistance that significantly reduces flow in the region.

The small variation observed in the particle adhesion curves for the 10 μm and 20 μm screens, along with their tendency to converge to the same final point (Fig. 11 A), indicates that both screens reach a state where all passages are obstructed relatively quickly. This observation is consistent with the similar velocity contours seen for these two screens in Fig. 10. In contrast, the 30 μm screen takes more time to accumulate a sufficient number of particles capable of obstructing all passages, leading to a more distinct behavior in its particle adhesion curve.

Although the screens exhibit similar behavior, especially the 10 μm and 20 μm screens, there is a significant increase in pressure drop as shown in Fig. 12. This can be attributed to the fact that the 10 μm screen allows for the adhesion of more smaller particles compared to the 20 μm screen, due to its smaller capture diameter.

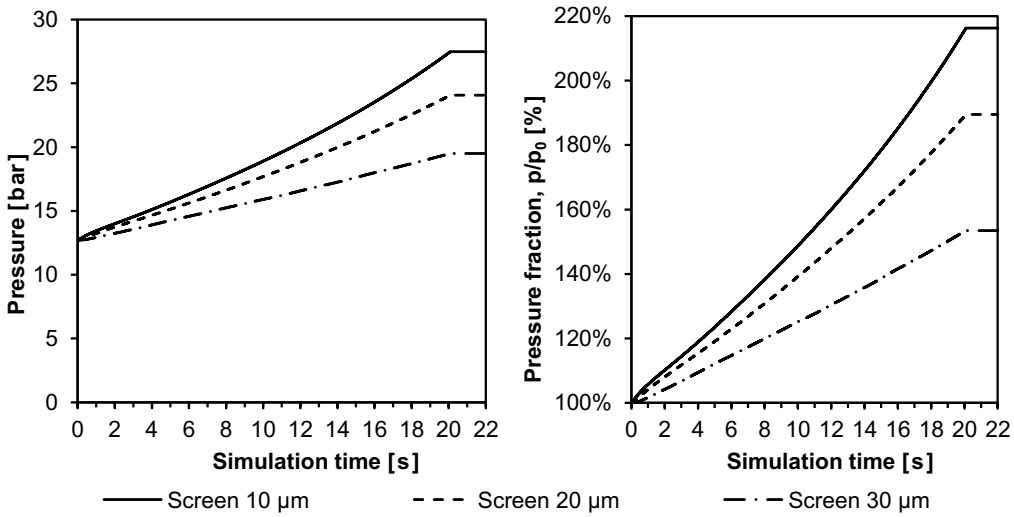

Figure 12: Pressure drop behavior of each screen.

The observed variation in pressure drop can be explained by the Ergun and Sauter equations (Equation 1), which consider the porosity and average diameter of the particles in the porous medium to determine the resistance and subsequent pressure drop. Despite having an approximate number of particles and flow advancement though the domain, as the 10 μm screen captures smaller particles since the beginning of the filtration process than the 20 μm screen, it has a lower mean diameter and porosity, resulting in a higher pressure drop.

4. Conclusion

Among the evaluated phenomena, the formation of a porous region due to particle agglomeration stood out, affecting both flow patterns and the adhesion of subsequent particles. The subroutines demonstrated satisfactory results, although they did not address all parameters that influence scaling, they exhibited consistent behaviors, such as changes in flow and particle adhesion as regions near the inlet, available for flow passage, became obstructed, resulting in flow redirection to other regions and an increase in pressure drop within the domain. The results showed that, for the same mass flow and particle dispersion, the screens tend to reach a similar flow state over time. This means that a less refined screen,

with a larger passage diameter, could be chosen due to the reduced cost compared to a more refined screen. However, the high particle concentration observed inside the production column before the formation of the second filtering layer could damage equipment. Another important observation was the significant increase in pressure drop with a reduction in screen passage diameter, which occurred due to the presence of finer particles that generate greater flow resistance when adhered to the screen surface. Therefore, for the same energy input, a smaller passage diameter would result in higher productivity losses. Despite the simplifications adopted, this methodology proved promising and could potentially be applied in decision-making processes, providing quick results for selecting the most suitable screen model. As future proposals, it is suggested to implement other adhesion criteria, such as an energy analysis considering parameters that influence turbulent flows, experimental calibration of the resistance generated by the particle bed, consideration of the possibility of detachment of deposited particles that did not scale, and the use of the developed subroutine for re-injecting the particle on the other side of the screen for inorganic salt precipitation, adjusted the particle generation conditions.

5. ACKNOWLEDGEMENTS

We would like to express our gratitude to the Instituto Federal do Espírito Santo for their support in the presentation and publication of this work.

6. REFERENCES

Bernabe, Y., Brace, W. and Evans, B., 1982. "Permeability, porosity and pore geometry of hot-pressed calcite". *Mechanics of Materials*, Vol. 1, No. 3, pp. 173–183. ISSN 0167-6636. doi:https://doi.org/10.1016/0167-6636(82)90010-2.

Chen, P.C., Tai, C.Y. and Lee, K., 1997. "Morphology and growth rate of calcium carbonate crystals in a gas-liquid-solid reactive crystallizer". *Chemical engineering science*, Vol. 52, No. 21-22, pp. 4171–4177.

Cosmo, R.P., Pereira, F.A.R., Ribeiro, D.C., Barros, W.Q. and Martins, A.L., 2019. "Estimating CO2 degassing effect on CaCO3 precipitation under oil well conditions". *Journal of Petroleum Science and Engineering*, Vol. 181. doi: 10.1016/j.petrol.2019.106207.

Cruz, S.F.R.D., 2018. *Modelagem matemática e simulação numérica da precipitação de carbonato de cálcio em condições de poço*. Mestrado em energia, Universidade Federal Do Espirito Santo, Espírito Santo.

Delta Screens, 2017. "Delta direct wrap on pipe screen". deltascreens.com/products/direct-wrap-on-pipe. Accessed 26 feb. 2023.

Ergun, S., 1952. "Fluid flow through packed columns". *Chemical Engineering Progress*, Vol. 48, pp. 89–94.

Maciel, R.S., Cruz, S.F.R., Pereira, F.A.R., Segantine, E.J., André, L.M. and Ferreira, M.V.D., 2020. "Numerical investigation of calcium carbonate scale at sliding sleeve valves for well completion". In *18th Brazilian Congress of Thermal Sciences and Engineering*.

Malbrel, C., Procyk, A. and Cameron, J., 1999. "Screen sizing rules and running guidelines to maximise horizontal well productivity". *SPE European Formation Damage Conference*.

Pessoa, T.F.P., 2012. *Análise numérica de medidas de contenção de sólidos em rochas produtoras de óleo do brasil*. Graduação em engenharia civil, Pontifícia Universidade Católica Do Rio de Janeiro, Rio de Janeiro.

Poletto, V.G., Mazuroski, M.E., Martins, M.R., De Lai, F.C., Junqueira, S.L.d.M., Castro, B.B.d., Schwalbert, M.P., Martins, A.L. and Oliveira, P.G.O.d., 2022. "Modeling and simulation of internal control valve (icv) calcium carbonate scale formation". In *19th Brazilian Congress of Thermal Sciences and Engineering*. Bento Gonçalves - RS - Brazil.

Sauter, J., 1926. "Die grössenbestimmung der in gemischnebeln von verbrennungskraftmaschinen vorhandenen brennstoffteilchen". *Berlin SW*, Vol. 19.

Schiavi, M.T. and Hoffmann, W.A.M., 2015. "Cenário petrolífero: sua evolução, principais produtores e tecnologias". *RDBCI: Revista Digital de Biblioteconomia e Ciência da Informação*, Vol. 13, No. 2, pp. 259–278. doi: 10.20396/rdbci.v13i2.2104.

Vieira, J.H.S., 2021. *Estudo computacional dos efeitos da variação dos diâmetros de cristais de carbonato de cálcio na adesão em equipamentos de extração do petróleo*. Trabalho de conclusão de curso, Instituto Federal de Educação, Ciência e Tecnologia do Espírito Santo, Espírito Santo. Graduação em Engenharia Mecânica.

Zhang, Y. and Farquhar, R., 2001. "Laboratory determination of calcium carbonate scaling rates for oilfield wellbore environments". *Society of Petroleum Engineers Inc.*

7. RESPONSIBILITY NOTICE

The authors are solely responsible for the printed material included in this paper.